Available online at www.sciencedirect.com
ScienceDirect
Trans. Nonferrous Met. Soc. China 32(2022) 1031−1040
Transactions of Nonferrous Metals Society of China
www.tnmsc.cn

Electrochemical recycling of Pd and Ag from simulated high-level liquid waste

You-bin WANG[1,2], Rui ZOU[1,2], Yue-zhou WEI[1,2], Tsuyoshi ARAI[3], Toyohisa FUJITA[1,2]

1. School of Resources, Environment and Materials, Guangxi University, Nanning 530004, China;
2. Guangxi Key Laboratory of Processing for Non-ferrous Metal and Featured Materials, Guangxi University, Nanning 530004, China;
3. Department of Material Science and Engineering, Shibaura Institute of Technology, Tokyo 3-9-14, Japan

Received 23 February 2021; accepted 4 November 2021

Abstract: For the recycling of Pd and Ag from high-level liquid waste (HLLW), the electrochemical behaviors of Pd and Ag in the simulated HNO_3 solutions were investigated by cyclic voltammetry and potentiostatic deposition. Scanning electron microscopy (SEM) and X-ray diffraction (XRD) were used to observe the deposits morphology and to evaluate their composition. The results indicate that the formation of NO_2^- helps to dissolve Ag while Ag is electrodeposited. When Pd and Ag are electrodeposited together, more metals are gained in the same time, and the deposited Ag does not dissolve in this situation. The metals are electrodeposited completely at the potentials from −0.4 to −0.6 V (vs MSE) and the deposits contain Ag and PdH_x. The electrodeposition of Pd can boost hydrogen evolution, and then the reaction between H_2 and NO_2^- is sped up, thereby lowering the concentration of NO_2^- and inhibiting the dissolution of Ag.

Key words: electrodeposition; metals recovery; nitrite generation; promoting effect; morphology characteristics

1 Introduction

Palladium (Pd) is a critical element belonging to the platinum group metals, which has many excellent properties such as great ductility, strong hydrogen absorption capacity and high catalytic activity [1,2]. Pd plays irreplaceable role in various industrial applications owing to its unique properties, and hence demand growth for Pd is expected to be sustained [3]. However, the low abundance of the Pd in earth crust confines the resource extraction to a low level even through mining. Besides, Ag is also a noble metal mainly derived from mining, which is consumed in large quantities. Ag and Pd are applied to the manufacture of many catalyst materials, and their alloy also has wide application prospect in industry [3−6]. Unfortunately, the stocks can be depleted by continuous mining operation, and recycling these rare metals from high-level liquid waste (HLLW) is a more environmentally friendly alternative method than traditional mining [7]. The spent fuel produced after nuclear fission in nuclear electricity generation contains metal resources like Pd, Ag [8−13] and the other fission platinoids (FPs) [14,15]. After the PUREX process, these valuable metals are transferred to the HLLW for subsequent treatment [16,17]. However, in the vitreous solidification process of HLLW, separate phases are generated in the form of metals or alloys because of the poor intersolubility between the fission products and the glass melt. It can deteriorate the stability of the glass, which is harmful to the long-term storage of nuclear waste [18]. Thus, it is necessary to remove these

Corresponding author: You-bin WANG, Tel: +86-771-3232200, E-mail: wangyoubin@gxu.edu.cn
DOI: 10.1016/S1003-6326(22)65852-7

elements from HLLW beforehand [19].

The content of Ag (4.21×10^1 g/t-U) and Pd (8.49×10^2 g/t-U) in spent fuel reaches a relatively high level after fission, and the isotopes of Ag and Pd include ^{104}Pd (17 wt.%), ^{105}Pd (29 wt.%), ^{106}Pd (21 wt.%), ^{107}Pd (16 wt.%), ^{108}Pd (12 wt.%), ^{110}Pd (4 wt.%) and ^{109}Ag (100 wt.%) [3,19]. Most of the FPs are stable nuclides with short half-life, except for ^{107}Pd that has a half-life of 6.5×10^6 years and emits a weak β-ray with energy of 0.035 MeV [20]. Thus, the radioactivity of nuclides can be reduced to a low level after attenuation, which allows them to be recycled for industry application [21,22]. The recovery methods of Pd and Ag have been reported, such as solvent extraction [23], sorption [12,24] and ion exchange [25,26]. Apart from that, Ag and Pd can be easily reduced by electrolysis due to their high reduction potential, so electrodeposition is regarded as a promising recycling way [27−29].

The electrochemistry researches are mainly focused on the regeneration of Ag and Pd in nitric acid medium, because similar acidic condition is formed after the leaching of spent fuel. KIRSHIN and POKHITONOV [30] investigated the electrodeposition ratio of Pd from 1 mol/L HNO_3 solution, and more than 99% Pd was recovered by the cathodic electrodeposition. JAYAKUMAR et al [13,31] studied the electrochemical behavior of palladium in nitric acid medium, and the recovery ratio of Pd was limited to 40% on stainless steel electrode. It was reported that Ag and Pd could be electrodeposited together during the electrolysis of simulated HLLW [28]. However, the coelectrodeposition mechanism of Ag and Pd in nitric acid medium has not been well studied. In order to improve the recovery rate of Ag and Pd in spent fuel liquid waste, it is necessary to explore the electrochemical behavior of Ag and Pd in HNO_3 solution.

In this work, in order to explore the possibility of selective electrodeposition, the basic researches on electrolytic recovery were carried out in HNO_3 solution. Particularly, we put emphasis on electrode potential, electrolysis time and NO_2^- formation during the electrodeposition, and their influences were also discussed by various methods in details.

2 Experimental

Analytical-grade reagents of HNO_3 (Guanghua, Guangdong, China) and $NaNO_2$ (CRM, Beijing, China) were purchased. $Pd(NO_3)_2\cdot2H_2O$ (SCR, Shanghai, China) and $AgNO_3$ (Shenbo, Shanghai, China) were dissolved in 3 mol/L HNO_3, and ultrapure water was used during the preparation. In addition, the simulated HLLW was prepared according to previous studies [32,33].

All the electrochemical experiments were done through the electrochemical workstation (PARSTAT 4000 A, Ametek, USA). The experiments were carried out by using a three-electrode electrolyzer with a porous glass sand core acting as separator (Fig. 1). The other equipment included a graphite carbon rod (surface area: 1.9 cm^2) as the working electrode, a Pt plate as the counter electrode, and mercurous sulfate electrode (MSE) with a Luggin capillary as the reference electrode. The HNO_3 solution containing metallic ions was injected into the cathode chamber, and HNO_3 solution with the same concentration was injected into the anode chamber. Before the experiments began, the solution was purged with nitrogen to remove oxygen.

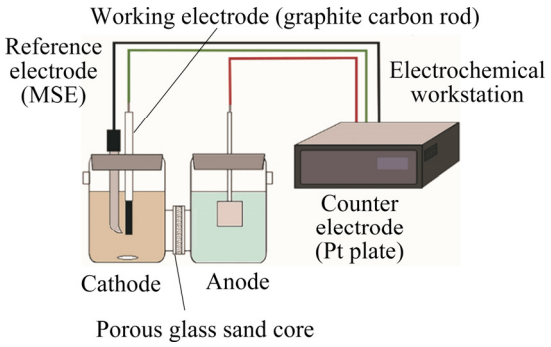

Fig. 1 Diagram of experimental apparatus

In the cyclic voltammetry experiments, the potential range was set to be from 0.8 to −0.7 V, and the scanning rate was 20 mV/s. The electrolytic reduction experiments were carried out at the potentials of −0.1, −0.2, −0.4 and −0.6 V (all potentials are displayed versus an Hg/Hg_2SO_4 electrode (MSE)). The ICP-AES (ICPS−7510, Shimadzu, Japan) was used to determine the concentration of metal elements in the solution. The UV−Vis spectrometer (UV−3600, Shimadzu, Japan) was used to determine the concentration of NO_2^- through ethanediamine photometry.

After the electrodeposition, the deposits were washed with deionized water and then dried

in a vacuum drying oven for the subsequent characterization analysis. The morphology and element composition of the deposits were analyzed by SEM−EDS (ProX, Phenom, Netherlands) and XRD (D/MAX 2500 V, Rigaku, Japan).

3 Results and discussion

3.1 Cyclic voltammetry

The electrodeposition potentials of Pd(II) and Ag(I) in 3 mol/L HNO_3 are determined by cyclic voltammetry, and the results are shown in Fig. 2. Correspondently, the cyclic voltammogram (CV) of control experiment carried out in HNO_3 solution under the same conditions is displayed in Fig. 3.

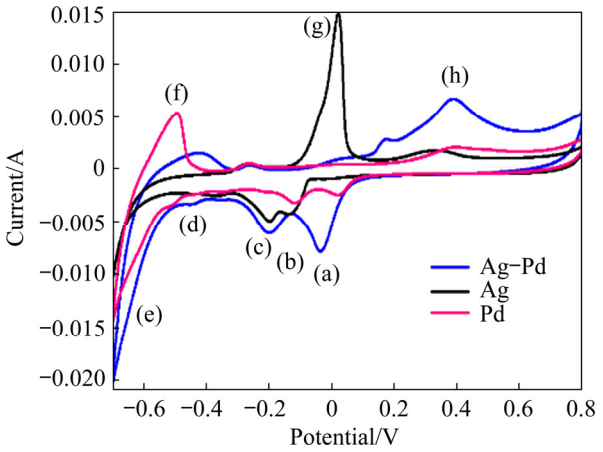

Fig. 2 Cyclic voltammograms of 10 mmol/L Pd(II), 10 mmol/L Ag(I) and 10 mmol/L Ag(I) + 10 mmol/L Pd(II) in 3 mol/L HNO_3 solution at 298 K with scan rate of 20 mV/s

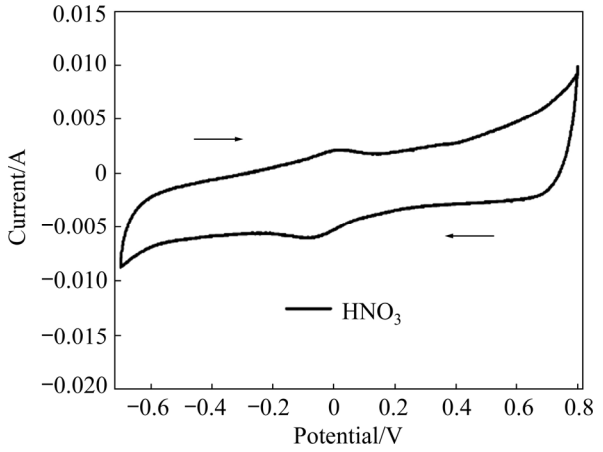

Fig. 3 Cyclic voltammogram of 3 mol/L HNO_3 solution at 298 K with scan rate of 20 mV/s

On the CV curve of Pd(II), the first reduction peak (a) appears at 0.10 V in the cathodic direction, which can be explained as the reduction from Pd(II) to Pd(0) (Reaction (1)) [1]. The reduction peak (b) at −0.10 V corresponds to the reduction from NO_3^- to NO_2^- (Reaction (2)) [28,34], which can also be seen from the CV curves of other HNO_3 solutions containing different solutes, as well as the pure HNO_3 solution. The weak reduction peak (d) at −0.45 V is related to the adsorption of H on metallic Pd (Reaction (3)) [34]. Then, the reduction current (e) caused by hydrogen evolution is visible in the cathodic sweep around −0.5 V, which is accompanied by many bubbles forming in experiments (Reaction (4)). During the positive scan, a large oxidation peak (f) at −0.48 V suggests the desorption of H from Pd, and the broad oxidation peak (h) occurring at 0.4 V indicates the oxidation of Pd(0) to Pd(II) [34].

$$Pd^{2+}\rightarrow Pd^0\ (\varphi_0=0.915\ \text{V vs NHE}) \quad (1)$$

$$2H^+ + NO_3^- + 2e \rightarrow NO_2^- + H_2O\ (\varphi_0=0.94\ \text{V vs NHE}) \quad (2)$$

$$Pd + xH^+ + xe \rightarrow PdH_x \quad (3)$$

$$2H^+ \rightarrow H_2\ (\varphi_0=0\ \text{V vs NHE}) \quad (4)$$

As is noticed on the CV curve of Ag(I), the reduction peak at −0.1 V is associated with the reduction of NO_3^-, as described in Reaction (2). The reduction peak (c) is assumed to be the reduction of Ag(I) according to Reaction (5), and the reduction reaction proceeds simultaneously with the generation of NO_2^- thereafter [35]. An obvious oxidation peak (g) is observed at 0 V in the anodic scan, which is assigned to the oxidation of Ag [36].

$$Ag^+ + e \rightarrow Ag \quad (5)$$

As shown on the CV curve of Ag(I)−Pd(II), it is confirmed that the reduction current is much larger than that of both single-element solutions. Compared with the Pd(II) solution, the adsorption and desorption peaks between H and Pd are observed on the CV curve of Ag(I)−Pd(II) solution, but the peak current decreases. And the oxidation peaks of Ag and Pd coalesce into a wide oxidation peak in this situation.

Moreover, it is seen that the hydrogen evolution reaction begins at −0.6 V in Ag(I) solution, while the hydrogen evolution potential drops down to about −0.45 V in the two other solutions containing Pd(II). It is supposed that the electrodeposition of Pd may bring about effect of electrocatalysis, and then the activation energy of

hydrogen evolution is reduced, causing that the hydrogen evolution reaction appears to happen at a low overpotential.

3.2 Potentiostatic electrolysis in Ag(I) and Pd(II) solution

The electrodeposition behavior of Ag(I) and Pd(II) in HNO_3 solution is investigated. As shown in Fig. 4, the electrodeposition ratio of Ag changes with increasing the electrolysis time under different potentials. Ag electrodeposition ratio (R_E) is calculated according to Eq. (6) [29]:

$$R_E=\frac{C_{Ag,0}-C_{Ag,t}}{C_{Ag,0}}\times 100\% \quad (6)$$

where $C_{Ag,0}$ and $C_{Ag,t}$ are the concentrations of Ag(I) ion at t=0 and at the time t, respectively.

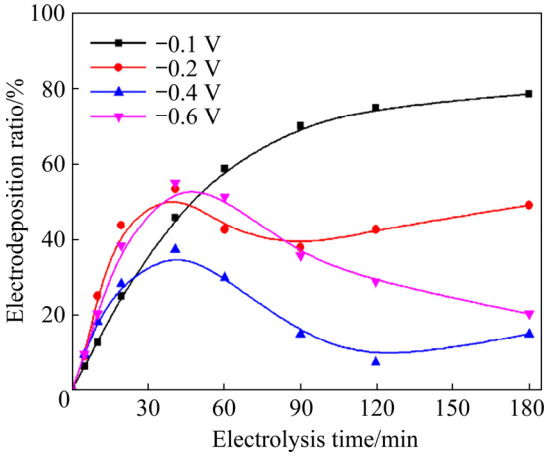

Fig. 4 Electrodeposition ratio of Ag in Ag(I) solution ([Ag(I)]=10 mmol/L; $C(HNO_3)$=3 mol/L; Potential: from −0.1 to −0.6 V (vs MSE))

As shown in Fig. 4, the electrolysis proceeds well at the potential of −0.1 V, and about 80% Ag has been recovered from the solution after 180 min. On the other hand, when the electrolytic potential is more negative than −0.2 V, the electrodeposition ratio reaches the maximum after 40 min and begins to decrease subsequently.

The amount of NO_2^- produced in Ag(I) solution is shown in Fig. 5, and the concentration of NO_2^- in the solution is very low at the potential of −0.1 V. However, the concentration of NO_2^- increases significantly after electrolysis for 40 min under the potentials higher than −0.2 V. It is inferred that the NO_2^- produced by reduction reaction acts as a self-catalyst, resulting in a sharp rise of its concentration [34].

By combining Fig. 4 with Fig. 5, it is seen that the electrodeposition ratio of Ag does not decline when there is only little NO_2^- in the solution. On the contrary, with the concentration of NO_2^- in the solution increasing, the amount of deposited Ag decreases to varying extents after a period of time. The electrodeposition of Ag is impeded because the NO_2^- in solution accelerates the dissolution of Ag, and the reaction equation is shown as Reaction (7). Therefore, in order to improve the electrodeposition ratio of Ag in HNO_3 solution, it is necessary to inhibit the formation of NO_2^-.

$$2Ag+4HNO_2\rightarrow 2AgNO_2+2H_2O+2NO \quad (7)$$

Figure 6 shows the variation of the Pd electrodeposited ratio as electrolysis time increases, and correspondingly the change in concentration of NO_2^- is shown in Fig. 7. It can be seen from Fig. 6 that the electrodeposition ratio of Pd increases as

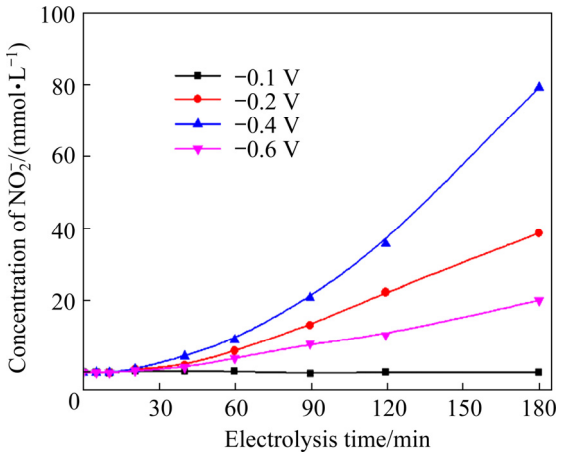

Fig. 5 Concentration change of NO_2^- during electrolysis in Ag(I) solution ([Ag(I)]=10 mmol/L; $C(HNO_3)$=3 mol/L; Potential: from −0.1 to −0.6 V (vs MSE))

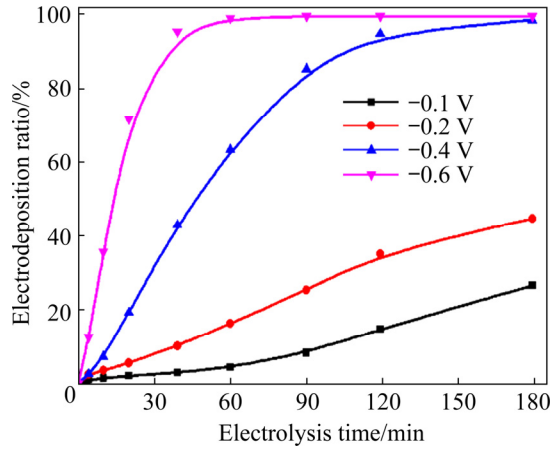

Fig. 6 Electrodeposition ratio of Pd in Pd(II) solution ([Pd(II)]=10 mmol/L; $C(HNO_3)$=3 mol/L; Potential: from −0.1 to −0.6 V (vs MSE))

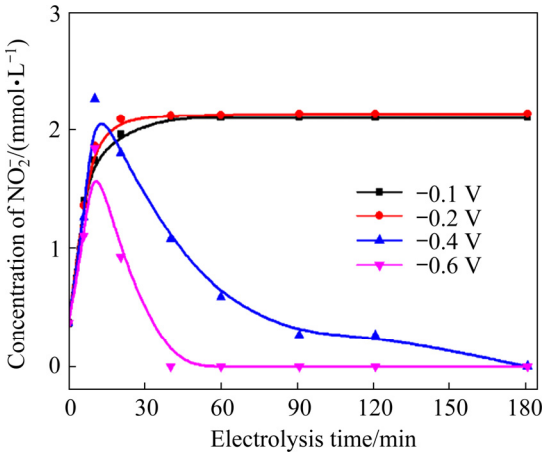

Fig. 7 Concentration change of NO_2^- during electrolysis in Pd(II) solution ([Pd(II)]=10 mmol/L, $C(HNO_3)$= 3 mol/L; Potential: from −0.1 to −0.6 V (vs MSE))

the reduction potential increases, and the electrodeposited ratio of Pd reaches higher than 95% at the potential of −0.6 V after electrolysis for 60 min. Compared with the reduction process of Ag(I), the redissolution phenomenon of deposited metal does not appear during the electrolysis of Pd(II) solution. As shown in Fig. 7, few NO_2^- is found during the electrolysis process. In addition, the concentration of NO_2^- decreases when solution is electrolyzed at −0.4 and −0.6 V, which means that the electrodeposition of Pd may be effective for inhibiting the formation of NO_2^-.

In order to understand the coelectrodeposition mechanism of Ag and Pd in HNO_3 solution further, the potentiostatic electrolysis of Ag(I)−Pd(II) solution is investigated.

As electrolysis time increases, the changes of the electrodeposited ratio and the concentration of NO_2^- are described in Fig. 8 and Fig. 9, respectively. Unlike the electrodeposition in Ag(I) solution, the electrodeposited Ag is not redissolved during the electrodeposition in Ag(I)−Pd(II) solution. Furthermore, it is confirmed that both Ag and Pd can be well electrodeposited at the potentials of −0.4 and −0.6 V, and nearly all the metals are recycled after electrolysis for 60 min.

Obviously, it is more easier to recycle Ag from Ag(I)−Pd(II) solution than Ag(I) solution. According to Fig. 9, there is few NO_2^- generated in the solution when the electrodeposition proceeds at the potentials of −0.4 and −0.6 V. By combining Fig. 8 with Fig. 9, it is speculated that the electrodeposition of Pd hinders the formation of NO_2^-, and promotes the electrodeposition of Ag indirectly in this process. Therefore, in order to improve the electrodeposition ratio of Ag, the coelectrodeposition of Ag and Pd is accepted as a beneficial way.

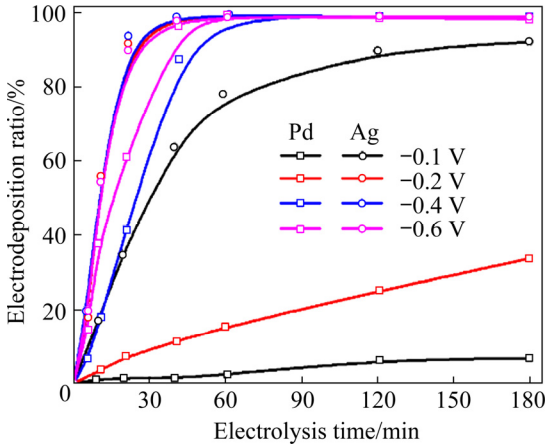

Fig. 8 Electrodeposition ratio of Ag and Pd in Ag(I)−Pd(II) solution ([Ag(I), Pd(II)]=10 mmol/L; $C(HNO_3)$=3 mol/L; Potential: from −0.1 to −0.6 V (vs MSE))

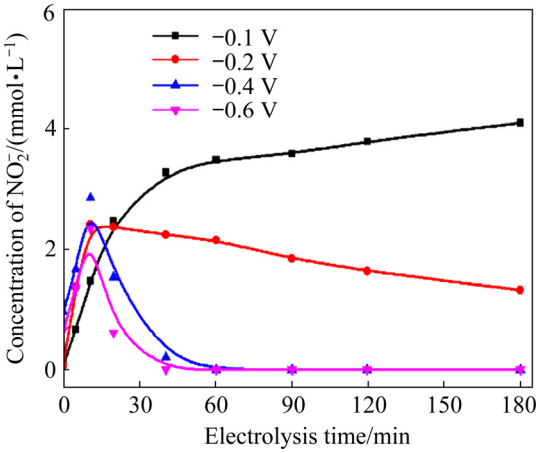

Fig. 9 Concentration change of NO_2^- during electrolysis in Ag(I)−Pd(II) solution ([Ag(I), Pd(II)]=10 mmol/L; $C(HNO_3)$=3 mol/L; Potential: from −0.1 to −0.6 V (vs MSE))

In order to explore the mechanism of the coelectrodeposition of Ag and Pd further, the analysis of the electrodeposition products acquired at the potentials of −0.1, −0.4 and −0.6 V is done. The morphology and composition of the deposits characterized by SEM, EDS and XRD are shown in Fig. 10 and Fig. 11.

The SEM−EDS images of the deposits obtained at different potentials from Ag(I)−Pd(II)

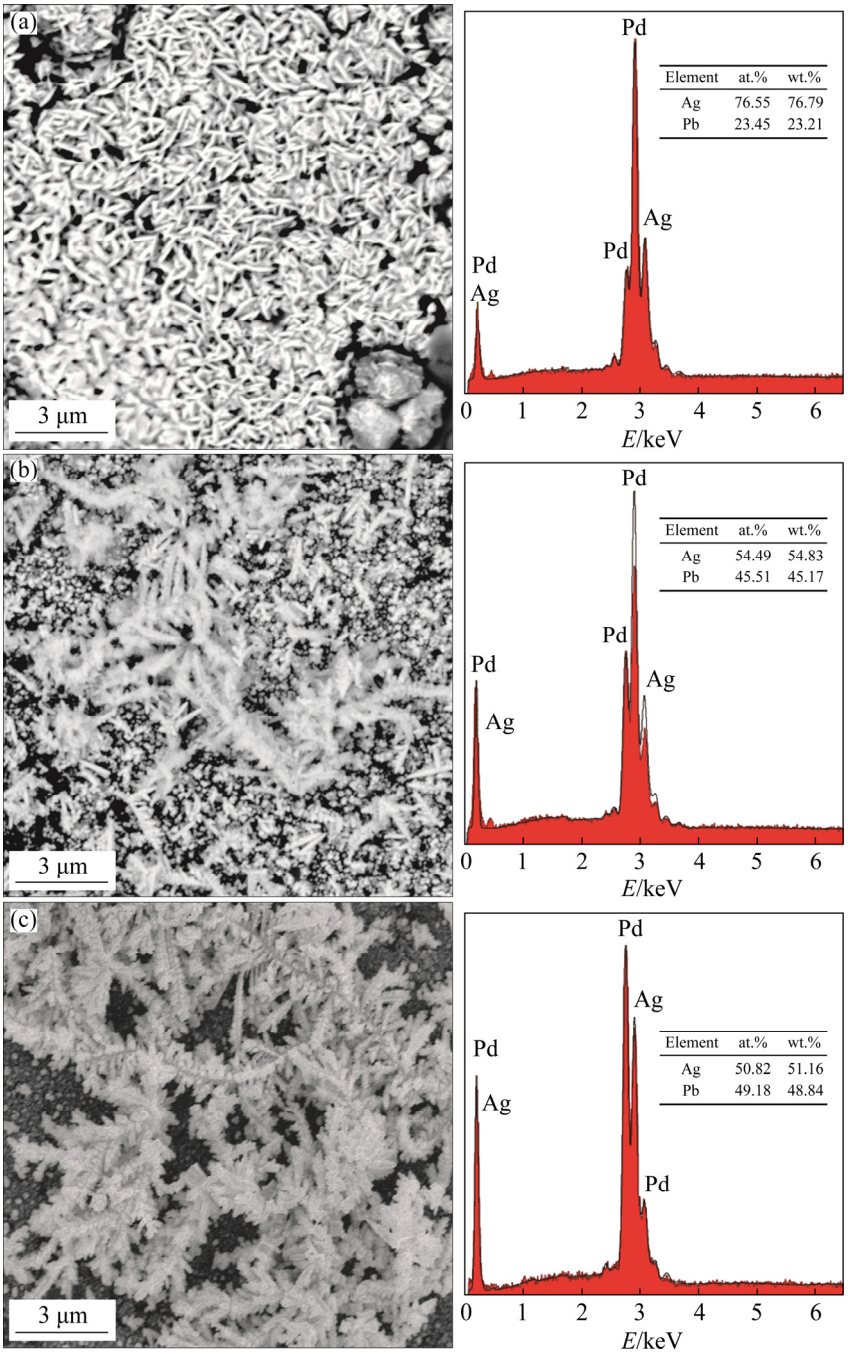

Fig. 10 SEM images and EDS analysis results of deposits obtained by electrolysis of Ag(I)−Pd(II) solution under different potentials (vs MSE) for 80 min: (a) −0.1 V; (b) −0.4 V; (c) −0.6 V

solution are displayed in Fig. 10. The deposits present to be a stacked sheet structure at −0.1 V (Fig. 10(a)), and the morphology of deposits appears to be dendritic at −0.4 V (Fig. 10(b)). As the overpotential becomes larger, the dendrites become bushier and have more slender bifurcations (Fig. 10(c)). The dendritic crystal structure always appears when metals with relatively low melting point such as Ag are electrodeposited [27]. It is seen that the morphology of deposits evolves from stacked sheet structure to pine-like shape with the potential increasing. The mass ratio of Ag to Pd is about 3:1 at −0.1 V, and the majority of the deposits on the substrate is Ag according to the EDS analysis. As a higher overpotential is applied, the Pd content of the deposits increases, which makes the mass ratio of Ag to Pd come to nearly 1:1 at −0.6 V. Therefore, it is inferred that Ag is initially deposited

in a certain shape, and then Pd is widely dispersed on the Ag crystal surface.

Combined with the result of XRD in Fig. 11, it is concluded that the deposits are Pd and Ag at −0.1 V, whereas the deposits are composed of PdH_x and Ag at −0.4 V. The composition of deposits has changed because Pd transforms into PdH_x (Reaction (3)).

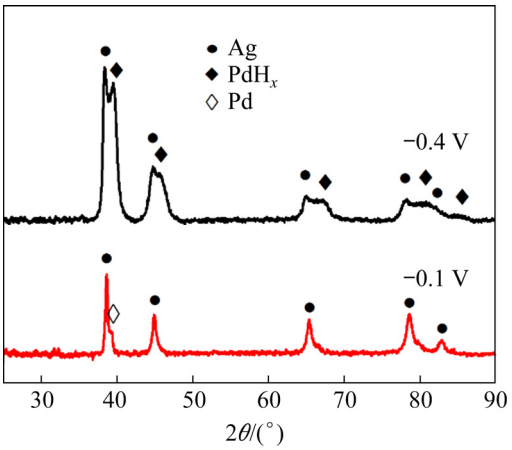

Fig. 11 XRD patterns of deposits obtained from Ag(I)−Pd(II) solution at −0.1 and −0.4 V (vs MSE)

3.3 Potentiostatic electrolysis in Pd(II)−NO_2^- solution

According to the previous results, the generation of NO_2^- is significantly restrained during the electrolysis when Pd is involved in the electrodeposition. In order to verify the mechanism further, the electrodeposited ratio of Pd and the concentration change of NO_2^- in Pd(II)−NO_2^- solution are studied.

As is described in Fig. 12, the electrodeposition rate of Pd increases as the reduction potential becomes higher. However, even it is under the same potential, obtaining the same recovery ratio needs more electrolysis time in Pd(II)−NO_2^- solution compared with the Pd(II) solution (Fig. 6). According to Fig. 13, the concentration of NO_2^- in the solution increases slightly with the electrodeposition time increasing at the potentials of −0.1 and −0.2 V, and the concentration of NO_2^- decreases drastically as the potential goes up to −0.4 V. It is inferred that the deposited PdH_x itself acts as an electrode, which enhances the hydrogen evolution reaction, accelerating the reaction between NO_2^- and H_2 eventually [1]. And the decomposition reaction of NO_2^- is speculated to be Reaction (8):

$$2HNO_2+H_2\rightarrow 2NO+2H_2O \quad (8)$$

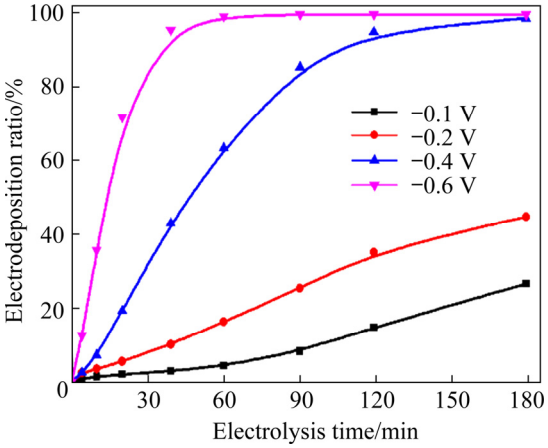

Fig. 12 Electrodeposition ratio of Pd in Pd(II)−NO_2^- solution ([Pd(II), NO_2^-]=10 mmol/L; $C(HNO_3)$=3 mol/L; Potential: from −0.1 to −0.6 V (vs MSE))

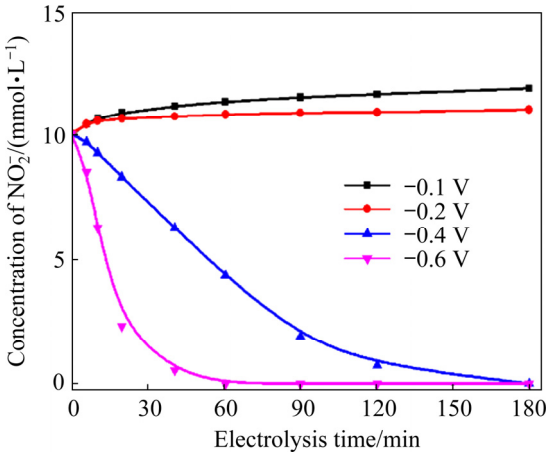

Fig. 13 Concentration change of NO_2^- during electrolysis in Pd(II)−NO_2^- solution: ([Pd(II), NO_2^-]=10 mmol/L; $C(HNO_3)$=3 mol/L; Potential: from −0.1 to −0.6 V (vs MSE))

3.4 Potentiostatic electrolysis in simulated HLLW

In fact, the real spent fuel waste has various side reactions during electrolysis due to the existence of assorted metallic elements [32,33], so it is necessary to study the effects of other elements.

According to Fig. 14, the electrodeposition of Ag and Pd also proceeds well at −0.4 V in the simulated solution, and about 70% Ag and 80% Pd have been recovered after electrolysis for 3 h. However, the electrodeposition speed is slower in the simulated liquid waste compared with HNO_3 solution (Fig. 8), which may be affected by other symbiotic elements in the simulated solution. In the simulated HLLW, Mo is considered to exist as binuclear complexes in the solution [37], and it has

different valence states according to the acidity and alkalinity of the solution, so the complexes of Mo existing in the electrolyte may be complicated. Similarly, a variety of complicated nitro complexes of Ru can be formed in HNO_3 solution [38]. These elements can hinder the electrodeposition of Ag and Pd in the simulated liquid waste. Thus, the interactions of these substances during electrolysis are worthy of note.

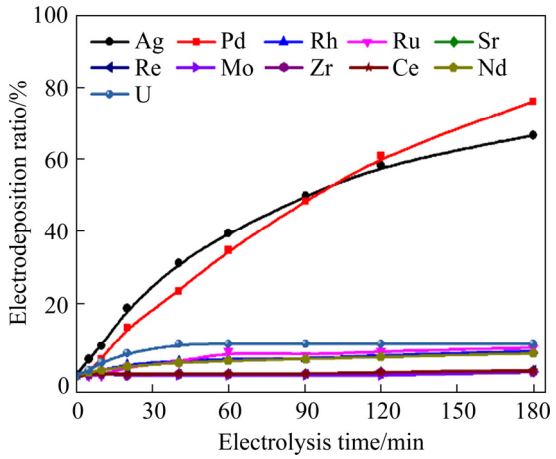

Fig. 14 Electrodeposition ratio of Ag and Pd in simulated liquid waste at potential of −0.4 V: ([Ag(I), Rh(III), Ru(III), Re(III), Zr(IV), Sn(II), Nd(III)]=0.5−1.5 mmol/L; [Pd(II), Ce(III)]=2.5−3.5 mmol/L; [Mo(VI)]=8.0 mmol/L; [U(VI)]=50 mmol/L; $C(HNO_3)$=3 mol/L; Potential: −0.4 V (vs MSE))

4 Conclusions

(1) In the Ag(I) solution, Ag can be well recycled through electrodeposition at the potential of −0.1 V. When the reduction potential is higher than −0.2 V, the electrodeposition of Ag is hindered because part of the deposited Ag is redissolved due to the NO_2^- formed during electrolysis.

(2) When it comes to the coelectrodeposition of Ag and Pd, it is confirmed that the deposition of Pd can inhibit the generation of NO_2^-, and make it possible for Ag to be completely electrodeposited in 30 min at lower potentials. This is because the hydrogen evolution is enhanced by the catalysis of Pd, which also helps speed up the reaction between H_2 and NO_2^-, eliminating the obstacle of Ag electrodeposition.

(3) According to the analysis of the deposits, Ag constitutes the majority of deposits at −0.1 V, whereas the Pd content in the deposits increases when a higher potential is applied. It is inferred that Ag initially deposits as sheet structure and then evolves into pine-like shape, while Pd is widely dispersed on the Ag crystal surface.

(4) In addition, it is confirmed that Ag and Pd can be well electrodeposited from the simulated HLLW simultaneously, and about 70% Ag and 80% Pd have been recovered after electrolysis for 3 h.

Acknowledgments

The authors are grateful for the financial supports from the National Natural Science Foundation of China (No. 11975082).

References

[1] LIU Sheng-chu, LIU Rui-qin, WU Yan, WEI Yue-zhou, FANG Bai-zeng. Study on electrochemical properties of palladium in nitric acid medium [J]. Energy Procedia, 2013, 39: 387−395. https://doi.org/10.1016/j.egypro.2013.07.227.

[2] CHRISTIAN A, ANNY J. Mechanistic and kinetic studies of palladium catalytic systems [J]. Journal of Organometallic Chemistry, 1999, 576(1): 254−278. https://doi.org/10.1016/S0022-328X(98)01063-8.

[3] KOLARIK Z, RENARD E V. Potential applications of fission platinoids in industry [J]. Platinum Metals Review, 2005, 49(12): 79−90. https://doi.org/10.1595/147106705X35263.

[4] MARECI D, SUTIMAN D, CAILEAN A, BOLAT G. Comparative corrosion study of Ag−Pd and Co−Cr alloys used in dental applications [J]. Bulletin of Materials Science, 2010, 33(4): 491−500. https://doi.org/10.1007/s12034-010-0075-z.

[5] KWON Jung-dae, LEE Sung-hun, LEE Koo-hyun, RHA Jong-joo, NAN Kee-seok, KWON Se-hun. Lubrication properties of silver-palladium alloy prepared by ion plating method for high temperature stud bolt [J]. Transactions of Nonferrous Metals Society of China, 2011, 21(S): s12−s16. https://doi.org/10.1016/S1003-6326(11)61052-2.

[6] KWON J D, LEE S H, LEE K H, RHA J J, NAM K S, CHOI S H, LEE D M, KIM D I. Silver−palladium alloy deposited by DC magnetron sputtering method as lubricant for high temperature application [J]. Transactions of Nonferrous Metals Society of China, 2009, 19(4): 1001−1004. https://doi.org/10.1016/ S1003-6326(08)60395-7.

[7] MUDD G M. Sustainability reporting and the platinum group metals: A global mining industry leader? [J]. Platinum Metals Review, 2012, 56: 2−19. https://doi.org/10.1595/147106711X614713.

[8] EDGAR C B, EDWARD J M, BRUCE K M, CHUCK Z S, JON M S. Sequestration of radioactive iodine in silver-palladium phases in commercial spent nuclear fuel [J]. Journal of Nuclear Materials, 2016, 482: 229−235. https://doi.org/10.1016/j.jnucmat.2016.10.029.

[9] STÉPHANE B, CHRISTOPHE P. Could spent nuclear fuel be considered as a non-conventional mine of critical raw materials? [J]. Progress in Nuclear Energy, 2017, 94: 222−

228. https://doi.org/10.1016/j.pnucene.2016.08.004.

[10] IGA Z, MICHAŁ Z, MICHAŁ P, ANDRZEJ P. Ruthenium as an important element in nuclear energy and cancer treatment [J]. Applied Radiation and Isotopes, 2020, 162: 109176. https://doi.org/10.1016/j.apradiso.2020.109176.

[11] ZOU Qing, GU Shuai, LIU Rui-qin, NING Shun-yan, CHEN Yan-liang, WEI Yue-zhou. Extraction chromatography–electrodeposition (EC−ED) process to recover palladium from high-level liquid waste [J]. Nuclear Science and Techniques, 2017, 28: 175. https://doi.org/10.1007/s41365-017-0327-3.

[12] NING Shun-yan, ZHANG Shi-chang, ZHANG Wei, ZHOU Jie, WANG Si-yi, WANG Xin-peng, WEI Yue-zhou. Separation and recovery of Rh, Ru and Pd from nitrate solution with a silica-based IsoBu-BTP/SiO_2−P adsorbent [J]. Hydrometallurgy, 2020, 191: 105207. https://doi.org/10.1016/j.hydromet.2019.105207.

[13] JAYAKUMAR M, VENKATESAN K A, SUDHA R, SRINIVASAN T G, RAO P R V. Electrodeposition of ruthenium, rhodium and palladium from nitric acid and ionic liquid media: Recovery and surface morphology of the deposits [J]. Materials Chemistry and Physics, 2011, 128(1/2): 141−150. https://doi.org/10.1016/j.matchemphys.2011.02.049.

[14] LIU Shi-jie. An unusual potential resource of platinum group metals−"fission platinoids (FPs)" from nuclear waste materials [J]. Precious Metals, 2013, 34(4): 60−64. http://en.cnki.com.cn/Article_en/CJFDTOTAL-GJSZ201304017.htm.

[15] ZDENEK K, EDOUARD V R. Recovery of value fission platinoids from spent nuclear fuel−Part II: Separation processes [J]. Platinum Metals Review, 2003, 47(3): 123−131. https://www.technology.matthey.com/article/47/3/123-131/.

[16] DAKSHINAMOORTHY A, DHAMI P S, NAIK P W, DUDWADKAR N L, MUNSHI S K, DEY P K, VENUGOPALB V. Separation of palladium from high level liquid waste of PUREX origin by solvent extraction and precipitation methods using oximes [J]. Desalination, 2008, 232(1−3): 26−36. https://doi.org/10.1016/j.desal.2007.11.052.

[17] POKHITONOV Y A, ROMANOVSKII V N. Palladium in irradiated fuel: Are there any prospects for recovery and application? [J] Radiochemistry, 2005, 47(1): 1−13. https://doi.org/10.1007/s11137-005-0040-7.

[18] KAZUYOSHI U, KAYO S, YOUICHI E, ICHIRO Y. Vitrification of high-level radioactive waste considering the behavior of platinum group metals [J]. Progress in Nuclear Energy, 2008, 50(2): 514−517. https://doi.org/10.1016/j.pnucene.2007.11.036.

[19] WEI Yue-zhou, TSUYOSHI A, HARUTAKA H, MIKIO K, AIMÉ B, PATRICK G. Development of a new aqueous process for nuclear fuel reprocessing: Hot tests on the recovery of U and Pu from a nitric acid solution of spent LWR fuel [J]. Nuclear Technology, 2005, 149(2): 217−231. https://doi.org/10.13182/NT05-A3591.

[20] ZDENEK K, EDOUARD V R. Recovery of value fission platinoids from spent nuclear fuel. Part I: General considerations and basic chemistry [J]. Platinum Metals Review, 2003, 47: 74−87. https://www.technology.matthey.com/pdf/pmr-v47-i2-074-087.pdf.

[21] GEORGE A J, A M P, GEORGE B M, WILLIAM J B. Recovery of noble metals from fission products [J]. Nuclear Technology, 1984, 65(2): 305−324. https://doi.org/10.13182/NT84-A33413.

[22] MASAKI O, YOSHIHIKO S, YUICHI S. The separation of fission-product rare elements toward bridging the nuclear and soft energy systems [J]. Progress in Nuclear Energy, 2002, 40(3): 527−538. https://doi.org/10.1016/S0149-1970(02)00047-1.

[23] MANIS K J, DIVIKA G, LEE Jae-chun, VINAY K, JEONG Jin-ki. Solvent extraction of platinum using amine based extractants in different solutions: A review [J]. Hydrometallurgy, 2014, 142: 60−69. https://doi.org/10.1016/j.hydromet.2013.11.009.

[24] SADYRBAEVA T Z. Membrane extraction and electrodeposition of silver(I) in systems with di(2-ethylhexyl) hydrogen phosphate [J]. Russian Journal of Applied Chemistry, 2007, 80(11): 1865−1870. https://doi.org/10.1134/S1070427207110171.

[25] SADYRBAEVA T Z. Liquid membrane system for extraction and electrodeposition of silver(I) [J]. Journal of Electroanalytical Chemistry, 2010, 648(2): 105−110. https://doi.org/10.1016/j.jelechem.2010.08.006.

[26] KONONOVA O N, LEYMAN T A, MELNIKOV A M, KASHIRIN D M, TSELUKOVSKAYA M M. Ion exchange recovery of platinum from chloride solutions [J]. Hydrometallurgy, 2010, 100(3/4): 161−167. https://doi.org/10.1016/j.hydromet.2009.11.011.

[27] LJILJANA A, EVICA R I, VESNA M M, MIROSLAV M P, MARINA V, JASMINA S S, NEBOJŠA D N. Correlation between crystal structure and morphology of potentiostatically electrodeposited silver dendritic nanostructures [J]. Transactions of Nonferrous Metals Society of China, 2018, 28(9): 1903−1912. https://doi.org/10.1016/S1003-6326(18)64835-6.

[28] JAYAKUMAR M, VENKATESAN K A, SRINIVASAN T G, RAO P R V. Electrolytic extraction of palladium from nitric acid and simulated high-level liquid waste [J]. Desalination and Water Treatment, 2009, 12(1−3): 34−39. https://doi.org/10.5004/dwt.2009.948.

[29] PILLAI K C, CHUNG Sang-joon, MOON I. Studies on electrochemical recovery of silver from simulated waste water from Ag(II)/Ag(I) based mediated electrochemical oxidation process [J]. Chemosphere, 2008, 73(9): 1505−1511. https://doi.org/10.1016/j.chemosphere.2008.07.047.

[30] KIRSHIN M Y, POKHITONOV Y A. Recovery of Pd from spent fuel: 1. electrochemical recovery of palladium from nitric acid solutions [J]. Radiochemistry, 2005, 47(4): 365−369. https://doi.org/10.1007/s11137-005-0102-x.

[31] JAYAKUMAR M, VENKATESAN K A, SRINIVASAN T G, RAO P R V. Studies on the feasibility of electrochemical recovery of palladium from high-level liquid waste [J]. Electrochimica Acta, 2009, 54(3): 1083−1088. https://doi.org/10.1016/j.electacta.2008.08.034.

[32] YUICHI S, NAOKI S, MASAHIKO Y. Selective recovery of minor trivalent actinides from high level liquid waste by R-BTP/SiO_2-P adsorbents [J]. IOP Conference Series:

Materials Science and Engineering, 2010, 9: 012064. https://iopscience.iop.org/article/10.1088/1757-899X/9/1/012064.

[33] TOMAR B S, MURALI M S, GODBOLE S V, RADHAKRISHNAN K, GURBA P B. Characterization of high level liquid waste generated from reprocessing of power reactor spent fuel [J]. BARC Newsletter, 2011, 320: 12−16. https://www.osti.gov/etdeweb/biblio/22206261.

[34] LIU Sheng-chu, WEI Yue-zhou, LIU Rui-qin, FANG Bai-zeng. Electrochemical behavior and electrowinning of palladium in nitric acid media [J]. Science China Chemistry, 2013, 56(12): 1743−1748. https://doi.org/10.1007/s11426-013-4945-2.

[35] SUN Yun-kai, GIOVANNI Z. Phase separation in electrodeposited Ag−Pd alloy films from acidic nitrate bath [J]. Journal of the Electrochemical Society, 2019, 166(8): D339-D349. https://iopscience.iop.org/article/10.1149/2.1231908jes.

[36] CRESPO-YAPUR D A, ELIZONDO A S, HERRERA D, VIDEA M. Galvanostatic electrodeposition of silver nanoparticles: Nucleation and growth studies [J]. Materials today: Proceedings, 2020. https://doi.org/10.1016/j.matpr.2020.04.760.

[37] SHINTA W, TOSHIKAZU S, MASATO N, TOMOKO Y, JUN O. Chemical forms of molybdenum ion in nitric acid solution studied using liquid-phase X-ray absorption fine structure, ultraviolet–visible absorption spectroscopy and first-principles calculations [J]. Chemical Physics Letters, 2019, 723: 76−81. https://doi.org/10.1016/j.cplett.2019.02.049.

[38] PRAVATI S, MALLIKA C, SRINIVASAN R, MUDALI U K, NATARAJAN R. Separation and recovery of ruthenium: A review [J]. Journal of Radioanalytical and Nuclear Chemistry, 2013, 298(2): 781−796. https://doi.org/10.1007/s10967-013-2536-5.

从模拟高放射废液中电化学回收钯和银

王友彬[1,2]，邹 睿[1,2]，韦悦周[1,2]，Tsuyoshi ARAI[3], Toyohisa FUJITA[1,2]

1. 广西大学 资源环境与材料学院，南宁 530004；

2. 广西大学 广西有色金属及特色材料加工重点实验室，南宁 530004；

3. Department of Material Science and Engineering, Shibaura Institute of Technology, Tokyo 3-9-14, Japan

摘 要：为从高放射废液(HLLW)中回收钯和银，采用循环伏安法和恒电位沉积法研究钯和银在模拟硝酸溶液中的电化学行为。利用扫描电子显微镜(SEM)和 X 射线衍射仪(XRD)观察沉积产物的形貌并分析其组成。结果表明，在单独电沉积银时亚硝酸根的生成促进银的溶解。当同时电沉积钯和银时，相同时间内更多金属被沉积，且沉积的银没有再出现溶解。在−0.4 ~ −0.6 V (vs MSE)的电位下，溶液中的金属被完全电沉积回收，沉积物组成为银和氢化钯。钯的电沉积可以促进析氢，随后加速亚硝酸根和氢气之间的反应，使溶液中的亚硝酸浓度降低，从而抑制银的再溶解。

关键词：电沉积；金属回收；亚硝酸生成；促进作用；形貌特性

(Edited by Bing YANG)